

Z.B. WANG<sup>1,✉</sup>  
B.S. LUK<sup>1</sup>, YANCHUK<sup>2</sup>  
L. LI<sup>1</sup>  
P.L. CROUSE<sup>1</sup>  
Z. LIU<sup>3</sup>  
G. DEARDEN<sup>4</sup>  
K.G. WATKINS<sup>4</sup>

# Optical near-field distribution in an asymmetrically illuminated tip–sample system for laser/STM nanopatterning

<sup>1</sup> Laser Processing Research Centre, School of Mechanical, Aerospace and Civil Engineering, University of Manchester, Sackville Street, Manchester M60 1QD, UK

<sup>2</sup> Data Storage Institute, DSI Building, 5 Engineering Drive 1, Singapore 117608, Singapore

<sup>3</sup> Corrosion and Protection Centre, School of Materials, University of Manchester, The Mill, Manchester M60 1QD, UK

<sup>4</sup> Laser Group, Department of Engineering, University of Liverpool, Brownlow Street, Liverpool L69 3GH, UK

Received: 5 December 2006 / Accepted: 2 May 2007  
Published online: 21 June 2007 • © Springer-Verlag 2007

**ABSTRACT** In surface nano-patterning using an atomic force microscope (AFM) tip in scanning tunnelling microscopy (STM) mode and illuminated by a laser, two controversial physical mechanisms exist in the literature: the field-enhancement (FE) model and the thermal-induced mechanical contact (TMC) model. Due to the presence of evanescent waves in the optical near-field, the exact calculation of the field distribution of the tip–sample system in micro/nano scales becomes complicated. There is a lack of understanding of the asymmetrically illuminated tip–sample system. In this paper, full 3D finite-difference time-domain (FDTD) analysis was carried out to investigate the field distribution in different tip–sample systems. The effects of different tip/sample materials (either dielectric or plasmonic material), the gap distance, and laser incidence angles on the field distribution/enhancement have been studied. For the first time, we have demonstrated two new effects which are helpful in distinguishing the controversial mechanisms: (1) on the sample surface, the field peak position has a shift away from the tip-axis at large angles of incidence, and (2) the field enhancement could depend strongly on the horizontal component (perpendicular to tip-axis) of the incident wave instead of the vertical component (along tip-axis). The optimal incident angle is around 30° for the maximum field under the tip. The existence of field-distribution nodes on the 3D tip surface that leads to the in-homogenous heating of the tip is also predicted.

PACS 81.16.Mk; 61.80.Ba; 81.16.Rf; 81.65.Cf

## 1 Introduction

To produce surface features with lateral dimensions below the conventional far-field diffraction limit, many near-field techniques have been developed in recent years, e.g., plasmonic lithography [1, 2], near-field optical scanning (NSOM) patterning [3, 4], laser-assisted particle-lens patterning [5–7] and laser-assisted tip patterning etc. [8–11]. In 1994, Gorbunov & Pompe published the first paper on the thin film nano-processing by laser/STM combination [9]. After

that, the technique was adopted by a number of researchers and was successfully applied to processing a variety of materials including metals, semiconductors and dielectrics. Despite of its wide applications, the physical mechanism behind the technique is still not clear. Two mechanisms have been proposed in the literature: (1) the field-enhancement (FE) model, where the enhanced optical field in the vicinity of the tip induces phase changes in the underlying substrate material [9–13]; and (2) the thermally induced mechanical contact (TMC) model, in which the laser-heat induced thermal expansion of the tip leads to mechanical contact between tip and substrate [8, 14]. In principle, the physical mechanism can be clarified by solving the coupled transient equations of electrodynamics (light interaction with tip–sample system), thermodynamics (temperature distribution of tip–sample system due to laser heating) and structural-dynamics (tip–sample expansion and cooling process). The complete theoretical analysis, however, seems to be quite complicated and has not been solved successfully. In the early period of laser/STM technique, authors like Gorbunov et al. [9] and Jersch et al. [10–12] were in favour of the FE model. They ignored or even ruled out the thermal effects of pulsed laser heating of the tip–sample system. This initiated several investigations of the thermal-induced tip expansion under nanosecond or femtosecond pulsed laser irradiation by Lyubinetzky et al. [15], Boneberg et al. [8] and Huber et al. [14]. They reported similar experimental and theoretical findings, viz. that the mechanical contact between the tip and sample was established in a time scale of several tenths of micro-seconds ( $\mu\text{s}$ ) by monitoring the transient tunnelling current, which was induced by the short pulse laser irradiation, thus making the FE effect dispensable. Although Gerstner et al. have pointed out these experiments [8, 14, 15] were limited by the low-frequency response of the STM current preamplifier, and that the fine structure (at ns time scale) of the transient current signal could be missed [16], it looks readily acceptable by most authors in the field that the mechanical contact is always established due to the thermal expansion of the tip. This was even later confirmed and accepted by Jersch et al., who had been the main supporters of the FE model [17]. Their experiments in [17] also confirmed the existence of the fast transient current phase at a time scale down to several ten nanoseconds (ns), as pre-

✉ Fax: +44 161 306 3803, E-mail: zengbo.wang@gmail.com

dicted by Gerstner et al. [16], before the start of the slow transient current phase in the  $\mu\text{s}$  time scale. The FE effect was supposed to be responsible for the observed fast transient current phase and the tip-bending effect due to asymmetric laser heating, as emphasized in [16, 17]. Obviously, this brings one back to the fundamental questions: how is the incident field scattered by the tip-sample system; and how is the tip asymmetrically heated under laser illumination in a laser/STM combination system?

From the theoretical point of view, the optical near-field distribution in the whole illuminated tip-sample system is the first step toward the goal to clarify the mechanisms. The optical near-field distribution determines how the incident laser energy is coupled into the tip-sample system, and thus it affects how the tip and the substrate are heated (the source term for the heat equations) and expanded. An asymmetrical field distribution on the tip surface means inhomogeneous heating of the different parts of the tip, leading to a more complex thermal expansion process including the possible tip-bending effect mentioned above. The field distribution on the tip surface, however, has not been calculated exactly and most of the previous publications use simplifying approximations [16, 18, 19]. Due to the fact that the size of tip-sample system is comparable with or smaller than the laser wavelength, macroscopic or geometrical optics are no longer applicable. The field distribution of the system, thus, requires direct solution of the full set of Maxwell equations. The finite-difference in time-domain (FDTD) method is used in this paper. The field distributions around several different tip-sample systems were calculated. The results presented in the paper emphasize the importance of exact modelling of the optical near-field distribution in laser-assisted STM nanopatterning problems.

## 2 The FDTD model and simulations

There are several methods for numerically solving electromagnetic problems for an arbitrary geometry. Examples are the multiple multi-pole (MMP) technique [20], the Green's function method [21], the finite element method [22] and the finite difference time domain (FDTD) technique [23], all of which have been applied to solving problems in near-field optics (NFO). Within them, the FDTD technique has been most widely used in recent years, mainly because it can provide complete spectral response of the system in a single computational run. The FDTD method also incorporates retardation effects, which can be important for scattering objects having dimensions comparable or larger than the wavelength. Specifically, without including retardation, the effect of induced charges far from the apex cannot be correctly taken into account. The FDTD algorithm consists of discretizing the Maxwell equations on a 3D-grid and then, starting from a given initial condition, marching a set of iterative relations forward in time. Upon choosing a suitably refined computational grid, the corresponding numerical solution gives an accurate representation of the dynamics of the electromagnetic field. A full 3D FDTD software package (CST Microwave Studio 2006) was used in the paper [24]. The computational domain is rectangular with dimensions  $L_x$  (500–2000 nm),  $L_y$  (500–2000 nm),  $L_z$  (650–4000 nm). A perfectly matched

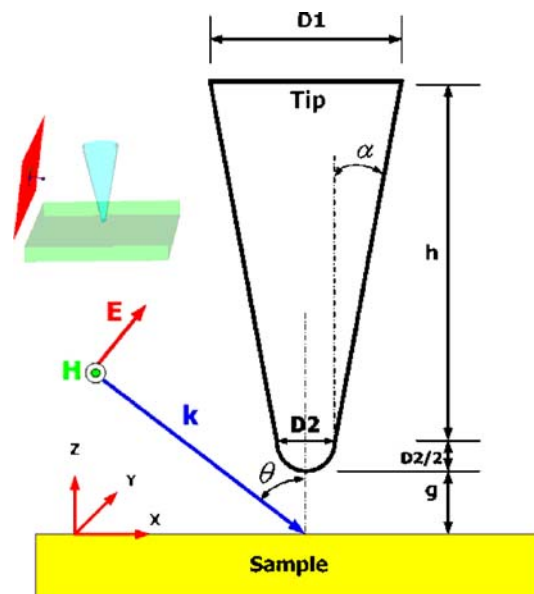


**FIGURE 1** Schematic of the tip-sample system simulated. The tip was modelled as a combination of a conical taper and a hemisphere of diameter  $D2$ . The opening angle of the tip is  $2\alpha$ .  $D1$  (diameter of the taper top),  $D2$  (diameter of the taper bottom) and  $h$  (height of the taper) was related by:  $D1 = D2 + 2h \tan(\alpha)$ . An electromagnetic plane wave of wavelength  $\lambda = 532 \text{ nm}$  angle  $\theta$ , with respect to the surface normal, and is polarized in the  $x$ - $z$ -plane

layer (PML) open boundary condition was applied for all the boundaries (numerical reflection coefficient  $< 0.01\%$  with a typical four-layered PML). Figure 1 shows the schematic of the tip-sample system studied in this paper. The tip is modelled as a conical taper terminated by a hemisphere with a curvature diameter of  $D2$ , which typically ranges from 20 nm to 120 nm. The tip opening angle is  $2\alpha$  in a range from  $10^\circ$ – $40^\circ$ . The base diameter of the tip  $D1$  is related to the opening angle and tip height  $h$  by:

$$D1 = D2 + 2h \tan(\alpha) . \quad (1)$$

The tip-sample has a separation distance,  $g$ , of several nanometres. A plane wave,  $\lambda = 532 \text{ nm}$ , is incident on the system at an oblique angle  $\theta$  with respect to the tip-axis ( $z$ -axis). The incident wave is polarized so that the electric vector,  $\mathbf{E}$ , lies in the  $x$ - $z$  plane. Four types of tip-sample systems were investigated and compared: (1) a dielectric-dielectric system (silicon tip-silicon sample); (2) dielectric-plasmonic system (silicon tip-gold sample); (3) plasmonic-dielectric system (gold tip-silicon sample); and (4) plasmonic-plasmonic system (gold tip-gold sample). The dielectric objects were meshed at a density of  $\lambda/10$  while the plasmonic objects were meshed at  $\lambda/30$ . The simulations were performed on a 64-bit, 16 GB memory, 3.2 GHz workstation. The optical constants of silicon and gold at 532 nm from Palik's book [25] were fitted by the Drude dielectric function:

$$\varepsilon(\omega) = \varepsilon_\infty - \frac{\omega_p^2}{\omega(\omega - i\gamma)} , \quad (2)$$

where  $\omega_p$  is the plasma frequency and  $\gamma$  the electron relaxation rate.  $\varepsilon_\infty$  includes the contribution of the bound electrons

Material	Dielectric constant at $\lambda = 532$ nm [25]	Drude fitting parameters
Silicon (Si)	$18.85 + 7.80i$	$\epsilon_\infty = 20, \omega_p = 2.60448 \times 10^{16}, \gamma = 2.40324 \times 10^{16}$
Gold (Au)	$-5.52 + 2.23i$	$\epsilon_\infty = 1, \omega_p = 9.56172 \times 10^{15}, \gamma = 1.21184 \times 10^{15}$

TABLE 1 Drude model fitting of parameters of silicon and gold

to the polarizability and equals 1 if only the conduction band electrons contribute to the dielectric function. Table 1 presents the fitted value of  $\epsilon_\infty, \omega_p$  and  $\gamma$  for Si and Au. It should be noted that the given Drude parameters in Table 1 are only valid for a narrow frequency region centred at 532 nm. It is suitable for the steady-state field distribution study in our problem. However, for spectral response studies, such parameters cannot be applied and an extended Drude model should be used [26].

### 3 Results and discussion

#### 3.1 Field distribution on the sample surface

We begin with the effect of different tip-sample system configurations ( $g, \theta$ , and materials varied) on the field

distribution on sample surface. The results are closely related to the FE mechanism model in the literature.

**3.1.1 Effect of the tip-sample gap distance.** A typical tip-sample geometry following [18], illustrated in Fig. 1, was used in the simulation ( $D_2 = 70$  nm,  $2^*\alpha = 25^\circ, \theta = 80^\circ$ ). The illumination length of the tip is  $\sim 25$   $\mu\text{m}$ . In the model this illumination length was truncated to several  $\mu\text{m}$ , due to the limited computational resources. The field distribution of the tip-sample system for different tip lengths ( $h = 300$  nm, 600 nm, 1200 nm and 3000 nm) was calculated and compared. It is found that the field distribution in the tip-sample gap region is qualitatively the same for  $h > \lambda$  (quantitatively,  $< 8\%$  numerical difference between the results for  $h = 600$  nm and  $h = 3000$  nm), which is in agreement with [27]. As far as the field distribution within the gap region is concerned, the tip

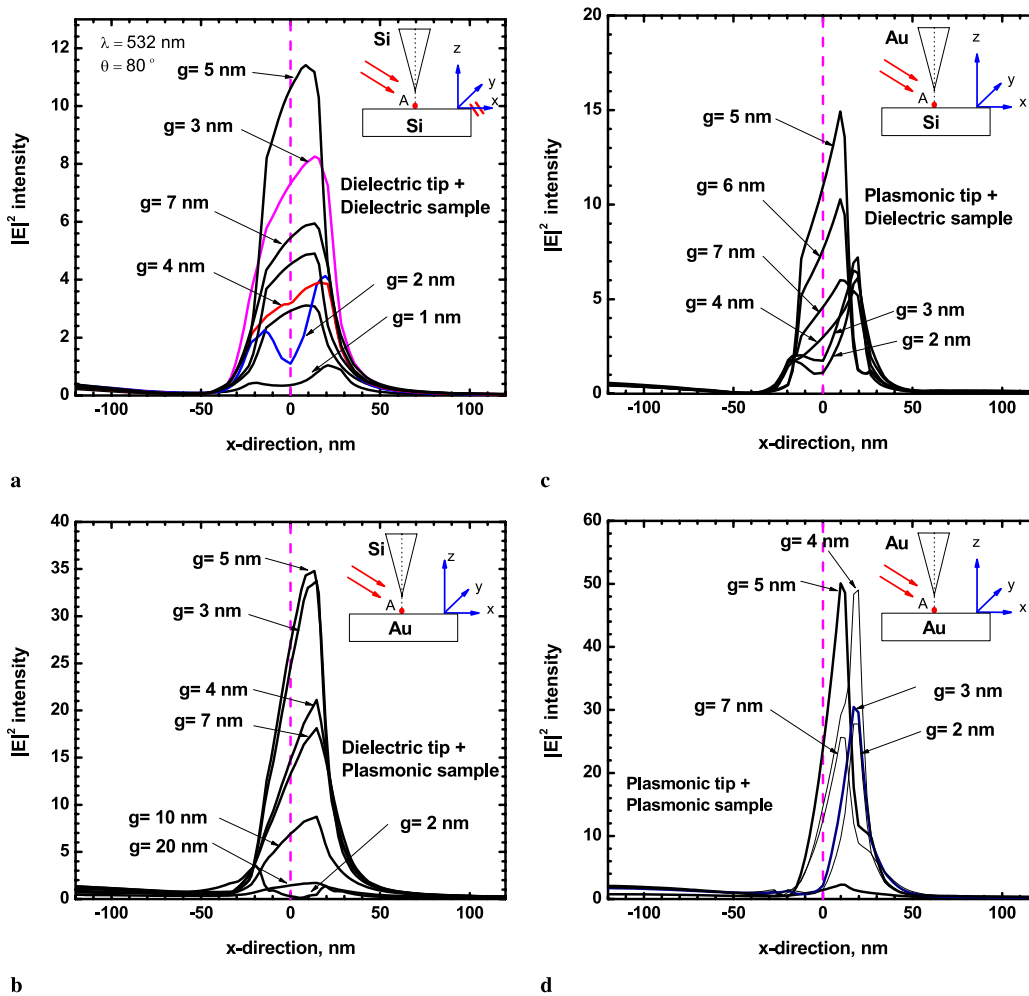
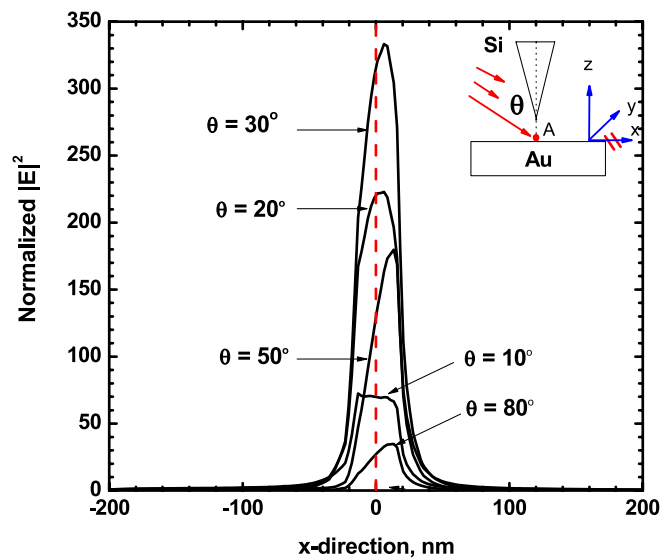


FIGURE 2 Normalized  $|E|^2$  intensity field distribution along  $x$ -direction on sample surface for four different tip-sample systems: (a) dielectric tip + dielectric sample system, (b) dielectric tip + plasmonic sample system, (c) plasmonic tip + dielectric sample and (d) plasmonic tip + plasmonic sample. The incident angle is fixed at  $80^\circ$

length of  $h = 600$  nm is thus sufficient to provide a comprehensive representation of the field structure. Figure 2 shows the normalized  $|E|^2$  intensity field distribution along the  $x$ -direction on the sample surface for the four tip-sample systems mentioned above. While keeping the laser incident angle fixed at  $80^\circ$ , the gap distance,  $g$ , was varied from 1 to 50 nm in the simulation. As can be seen in Fig. 2, the field maxima were reached at  $g = 5$  nm for all the four systems, which is independent of the materials of the tip and sample. As  $g$  increases further, the intensity drops quickly. At  $g \geq 20$  nm, almost no enhancement exists under the tip (for  $g \geq 20$ , all cases are similar to Fig. 2b). Since the tip-sample systems reach their field maxima at the same gap distance regardless of the material, it could be suggested the dominant resonance modes excited in the gap region depend mainly on the geometry of the tip-sample system, e.g., the hemisphere diameter, tip opening angle and incident angle [28]. In the dielectric-dielectric and dielectric-plasmonic systems as shown in Fig. 2a and b, two types of field profiles were observed: (1) double peak profiles with a central minimum for  $g = 1, 2$  nm; and (2) single peak profiles for  $g \geq 3$  nm. The field in the dielectric-plasmonic gap region (Fig. 2b) is extremely sensitive when the tip-sample distance is within  $2 \leq g \leq 3$  nm; a sudden increase of the field enhancement occurs for the 1-nm distance variation. In contrast, the field profiles in the plasmonic-dielectric and plasmonic-plasmonic system at  $g = 2$  nm and  $g = 3$  nm are almost the same, as shown in Fig. 2c and d. Under a typical STM tunnelling condition, the gap distance is  $\sim 1$  nm [17]. Due to the fluctuation of experimental conditions as well as the tip-expansion/contraction effect under the pulsed laser illumination, the gap distance has a high probability of oscillating between 1 nm and 3 nm. Thus, the field sensitivity in a dielectric-plasmonic system could account for the observed chaotic behaviour of the tunnelling current in the ns time scale [17]. Although the plasmonic material does not affect the geometrical resonance modes in the gap region, the plasmon resonance modes excited in the gold (Au) tip/sample (Fig. 2b–d) at  $\lambda = 532$  nm has increased the intensity of the field maxima as compared to the pure dielectric-dielectric system (Fig. 2a). An intensity peak of  $\sim 50$  can be seen in the plasmonic-plasmonic system in Fig. 2d at the position ( $x = 10$  nm,  $y = 0$  nm) on the surface when  $g = 5$  nm. It is noted the peak position of the field maxima are not at the tip-sample “contact” point ( $x = 0$  nm,  $y = 0$  nm, point A in the inset figures) but rather at a small distance  $\delta$  ( $5 \leq \delta \leq 20$  nm) away from the tip-axis in the  $x$ -direction. In a previous paper, we have shown the peak position shift effect for a  $1.0\text{-}\mu\text{m}$  spherical particle sitting on the sample surface, illuminated by an angular incident laser beam [29], both theoretically and experimentally. This effect, however, has not so far been reported in the literature for the experiments on nanopatterning by laser-tip combination method. Two reasons could account for this: (1) the shift distance  $5 \leq \delta \leq 20$  nm could easily have been missed during AFM measurement; and (2) the FE effect is not the dominant physical mechanism, and nano-structuring is instead caused by tip-sample mechanical contact as postulated by the thermal model. To identify the dominant mechanism, it is, thus, suggested that experimentalists in the field pay special attention to the location of nano-features relative to the position



**FIGURE 3** Normalized  $|E|^2$  intensity field distribution along  $x$ -direction on sample surface underneath the tip as a function of laser incident angle  $\theta$ . The maximum intensity is about 333 at  $\theta = 30^\circ$

of a tip apex after processing; an experimental observation of the position shift could provide direct proof of the FE model.

**3.1.2 Effect of the laser incident angle.** In the experiments the laser incident angle  $\theta$  was generally set as  $> 45^\circ$  following the literature (e.g.,  $73^\circ$  in [30],  $80^\circ$  in [17, 18], and  $90^\circ$  in [31]). The theoretical basis for doing so was established by Novotny et al. who showed it is crucial to have a large component of the excitation field along the axial direction, i.e., the vertical component  $E_z$ , to obtain a high field enhancement under the tip apex (the angle was set as  $90^\circ$  in their simulation [32]). It should be noted, however, the system studied by Novotny et al. contains only a tip and no substrate was taken into account. When a substrate is brought near to the tip, multiple reflections and scattering between them would take place and the field maximum was reached at some angle smaller than  $90^\circ$  [13], i.e., the horizontal component of the excitation field  $E_x$  plays a more important role. Martin et al. reported an angle of  $60^\circ$  for the field maximum [13].

Figure 3 shows the intensity distribution on the sample surface as a function of the laser incident angle at a fixed gap distance of  $g = 5$  nm, for the dielectric-plasmonic tip-sample system. All parameters, except the incident angle  $\theta$ , are the same as for Fig. 2b. The angle was scanned in a range from  $0^\circ$  to  $90^\circ$  with a step size of  $5^\circ$ . It is found that the maximum intensity,  $\sim 333$ , occurs at  $\theta = 30^\circ$ , which is much higher than the enhancement of  $\sim 35$  at  $\theta = 80^\circ$ . Calculations of the other three tip-sample systems (Fig. 2a,c,d) confirm the angle of  $\theta \approx 30^\circ$  is the optimal angle for all the four tip-sample systems, regardless of the tip/sample material. It is important to note that at the angle  $\theta \approx 30^\circ$  the horizontal component of the excitation field  $E_x$  exceeds the vertical component  $E_z$ . Based on this effect, experiments studying the effects of variation of the incident angle could be designed and carried out to determine the dominating mechanism.

3.2 Power loss density distribution (PLD) of the tip

We now turn our attention to the distribution of power loss density (PLD)

$$PLD = \frac{d}{dt} \left( \frac{dJ}{dV} \right) \quad (\text{Unit: W cm}^{-3}) \quad (3)$$

in the tip, which quantifies how the tip absorbs the incident power. This is closely related to the TMC mechanism model in the literature. In Fig. 4, the asymmetric field distribution in the  $x$ - $z$ -plane of the dielectric-plasmonic tip-sample system is given. The asymmetric field leads to the non-uniform illumination of the tip. The majority of the front side of the tip, as shown in Fig. 4b, is illuminated while the majority

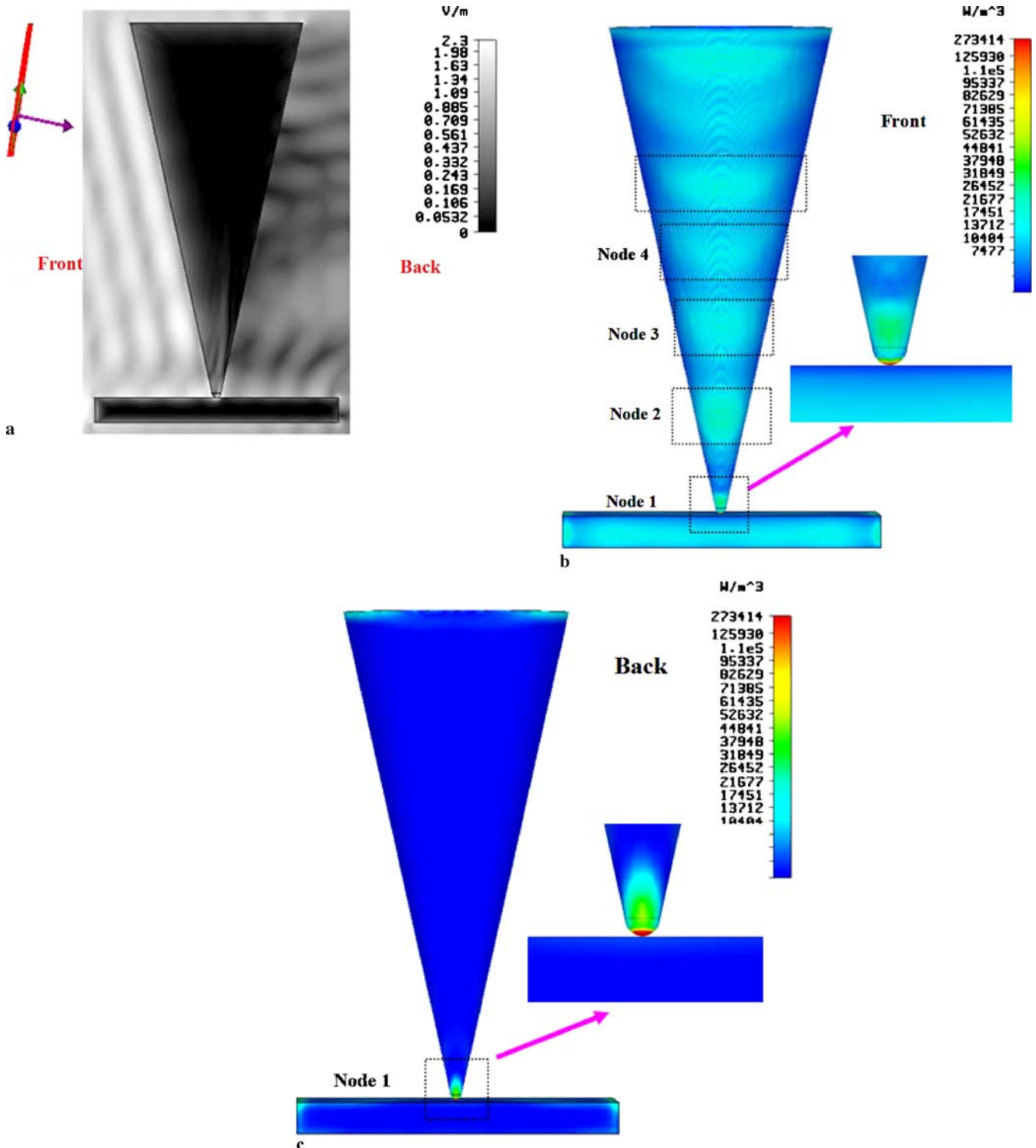


FIGURE 4 Normalized  $|E|$ -field distribution in the (a)  $x$ - $z$ -plane (incident  $E$ -vector is in this plane) at  $g = 1$  nm and corresponding (b) front and (c) back side view of the power loss density distribution of the simulated dielectric-plasmonic tip-sample system

of the back side of the tip (Fig. 4c) is shadowed. (Here the front side means the side facing the laser illumination). This is readily understandable from a conventional geometric optics point of view. However, at the front side of the tip the non-homogeneously scattered field leads to the laser energy being absorbed by the different parts of the tip surface, i.e., the existence of heating nodes as indicated in Fig. 4b (nodes 1, 2, 3, 4 ...) are predicted. At the back side of the tip as shown in Fig. 4c, only the very end of the tip is heated (node 1). The height of node 1 in both Fig. 4b and c is around 140 nm, i.e.,  $\sim 2D_2$ . Since both sides of the tip in the region of node 1 absorb similar amounts of laser energy (similar level of power loss density as seen in the inserts in Fig. 4b and c). This implies a nearly homogenous laser heating effect of the both sides of the very end of the tip, and thus the tip material in this region only expands/shrinks along the tip-axis. Tip-bending could only start from the node 2 region ( $\sim 500$  nm away from the tip apex), where asymmetrical absorption of laser energy appears for the front/back sides of the tip. Exact modelling of the transient temperature distribution under pulsed laser irradiation, by taking into account of the in-homogenous heating nature of the problem, is the next step work we are going to attempt.

Finally, the plasmon resonance excited in gold material under a 532 nm laser undergoes a high dissipative process. The field structure, however, could be changed dramatically in the case when a weakly absorbing plasmonic material is used [33, 34].

#### 4 Conclusions

The optical near-field distributions in the conical tip-sample systems have been investigated by the FDTD method. Calculations show the resonance modes excited in the tip-sample gap region to be affected purely by the geometry and to be independent of the material. The plasmon resonance helps to create a higher intensity in the optical near-field. We have identified two new effects in the conical tip-sample systems: (1) the peak shift effect, where the intensity peak position is found to be shifted away from the tip-axes; and, (2) the dominance of the horizontal component of the incident wave over its vertical component. These new effects can be utilized to design experiments to distinguish between the two controversial mechanisms. The existence of heating nodes on the 3D surface of the tip has also been demonstrated. This supports the non-homogenous heating effect of the tip under asymmetrical laser illumination.

**ACKNOWLEDGEMENTS** This research is funded by the UK North West Science Council (Grant No: N0003200). The authors would like to thank Mr. Zhou Yi at the Data Storage Institute, Singapore, for his help in

solving the technical issues regarding remote access of DSI's CST software from Manchester.

#### REFERENCES

- 1 W. Srituravanich, N. Fang, S. Durant, M. Ambati, C. Sun, X. Zhang, *J. Vac. Sci. Technol. B* **22**, 3475 (2004)
- 2 Z. Liu, Q. Wei, X. Zhang, *Nano Lett.* **5**, 957 (2005)
- 3 E. Betzig, J.K. Trautman, R. Wolfe, E.M. Gyorgy, P.L. Finn, M.H. Kryder, C.-H. Change, *Appl. Phys. Lett.* **61**, 142 (1992)
- 4 R. Riehn, A. Charas, J. Morgado, F. Cacialli, *Appl. Phys. Lett.* **82**, 526 (2003)
- 5 Z.B. Wang, M.H. Hong, B.S. Luk'yanchuk, S.M. Huang, Q.F. Wang, L.P. Shi, T.C. Chong, *Appl. Phys. A* **79**, 1603 (2004)
- 6 Y. Lu, S. Theppakuttai, S.C. Chen, *Appl. Phys. Lett.* **82**, 4143 (2003)
- 7 Y.F. Lu, L. Zhang, W.D. Song, Y.W. Zheng, B.S. Luk'yanchuk, *JETP Lett.* **72**, 457 (2000)
- 8 J. Boneberg, H.-J. Münzer, M. Tresp, M. Ochmann, P. Leiderer, *Appl. Phys. A* **67**, 381 (1998)
- 9 A.A. Gorbunov, W. Pompe, *Phys. Stat. Solidi A* **145**, 333 (1994)
- 10 J. Jersch, K. Dickmann, *Appl. Phys. Lett.* **68**, 868 (1996)
- 11 J. Jersch, F. Demming, K. Dickmann, *Appl. Phys. A* **64**, 29 (1997)
- 12 J. Jersch, F. Demming, L.J. Hildenhausen, K. Dickmann, *Appl. Phys. A* **66**, 29 (1998)
- 13 O.J.F. Martin, C. Girard, *Appl. Phys. Lett.* **70**, 705 (1997)
- 14 R. Huber, M. Koch, J. Feldmann, *Appl. Phys. Lett.* **73**, 2521 (1998)
- 15 I. Lyubinsky, Z. Dohnalek, V.A. Ukraintsev, J.J.T. Yates, *J. Appl. Phys.* **82**, 4115 (1997)
- 16 V. Gerstner, A. Thon, W. Pfeiffer, *J. Appl. Phys.* **87**, 2574 (2000)
- 17 J. Jersch, F. Demming, I. Fedotov, K. Dickmann, *Appl. Phys. A* **68**, 637 (1999)
- 18 S.M. Huang, M.H. Hong, Y.F. Lu, B.S. Luk'yanchuk, W.D. Song, T.C. Chong, *J. Appl. Phys.* **91**, 3268 (2002)
- 19 V.A. Ukraintsev, J.J.T. Yates, *J. Appl. Phys.* **80**, 2561 (1996)
- 20 C. Hafner, *The Generalized Multiple Multipole Technique for Computational Electromagnetics* (Artech, Boston, 1990)
- 21 O.J.F. Martin, C. Girard, A. Dereux, *Phys. Rev. Lett.* **74**, 526 (1995)
- 22 J.M. Jin, *The Finite Element Method in Electromagnetics*, 2nd edn. (Wiley, New York, 2002)
- 23 A. Taflov, *Computational Electrodynamics: The Finite-Difference Time-Domain Method* (Artech, Boston, 2005)
- 24 Computer Simulation Technology, CST Microwave Studio; Remote license access provided by one of the author B.S. Luk'yanchuk in DSI, Singapore (2006) (<http://www.cst.com>)
- 25 E.D. Palik, *Handbook of Optical Constants of Solids III* (Academic Press, New York, 1998)
- 26 A. Vial, A.-S. Grimault, D. Macías, D. Barchiesi, M.L. de la Chapelle, *Phys. Rev. B* **71**, 085416 (2005)
- 27 R.M. Roth, N.C. Panoiu, M.M. Adams, R.M. Osgood Jr., C.C. Neacsu, M.B. Raschke, *Opt. Express* **14**, 2921 (2006)
- 28 Z.B. Wang, L. Li, Z. Liu, B.S. Luk'yanchuk, P.L. Crouse, G. Dearden, K.G. Watkins, to be published (2007)
- 29 Z.B. Wang, M.H. Hong, B.S. Luk'yanchuk, Y. Lin, Q.F. Wang, T.C. Chong, *J. Appl. Phys.* **96**, 6845 (2004)
- 30 A. Kirsanov, A. Kiselev, A. Stepanov, N. Polushkin, *J. Appl. Phys.* **94**, 6822 (2003)
- 31 Y.F. Lu, B. Hu, Z.H. Mai, W.J. Wang, W.K. Chim, T.C. Chong, *Japan. J. Appl. Phys.* **40**, 4395 (2001)
- 32 L. Novotny, R.X. Bian, X.S. Xie, *Phys. Rev. Lett.* **79**, 645 (1997)
- 33 B.S. Luk'yanchuk, M.I. Tribelsky, V. Ternovsky, *J. Opt. Technol.* **73**, 371 (2006)
- 34 Z.B. Wang, B.S. Luk'yanchuk, M.H. Hong, Y. Lin, T.C. Chong, *Phys. Rev. B* **70**, 035418 (2004)